



Sliding Mode Speed Estimation of Induction Motor with MPC Based Flux Weakening Control for Electric Vehicle

*Makale Bilgisi / Article Info

Alındı/Received: 22.04.2024

Kabul/Accepted: 06.08.2024

Yayımlandı/Published: 02.12.2024

Elektrikli Araç için MÖK Tabanlı Akı Zayıflatma Kontrolü ile Asenkron Motorun Kayan Modlu Hız Tahmini

Bariş ÇAVUŞ* , Mustafa AKTAŞ 

Ondokuz Mayıs University, Engineering Faculty, Department of Electrical and Electronics Engineering, Samsun, Türkiye

© Afyon Kocatepe Üniversitesi

Abstract

It is very important to operate the motors used in electric vehicles above the rated speed. In order to operate electric motors with very high speed, the flux must be decreased in a controlled way. The Model Predictive Control (MPC) approach was employed in this study to reduce the flow. In the flux weakening area, the induction motor's performance without a speed sensor has been evaluated. As a result of the study, both the speed sensorless performance of the MPC based flux weakening control has been examined and performance of the Model Reference Adaptive System (MRAS) and the Sliding Mode Observer (SMO) in very high speed region over nominal value has been evaluated. It has been successfully demonstrated that MPC-based flux weakening control with two speed observers can be achieved based on the current, speed, flux, and torque data collected through the simulation study. In addition, as a result of the study, it is seen that SMO has given better results.

Keywords Model predictive control; Flux weakening; Model reference adaptive system; Sliding mode observer; Direct torque control.

Öz

Elektrikli araçlarda kullanılan motorların nominal hızın üzerinde çalıştırılması çok önemlidir. Elektrik motorlarının çok yüksek hızda çalıştırılabilmesi için akının kontrollü bir şekilde azaltılması gerekmektedir. Bu çalışmada akışı azaltmak için Model Öngörülü Kontrol (MÖK) yaklaşımı kullanılmıştır. Akı zayıflama bölgesinde hız sensörsüz asenkron motorun performansı değerlendirilmiştir. Çalışma sonucunda hem MÖK tabanlı akı zayıflatma kontrolünün hız sensörsüz performansı incelenmiş hem de Model Referans Adaptif Sistem (MRAS) ve Kayan Kipli Gözlemcinin (KKG) nominal değer üzerindeki hız bölgesinde performansı değerlendirildi. Benzetim çalışmasıyla elde edilen akım, hız, akı ve moment verilerine dayanarak iki hız gözlemcisi ile de MPC tabanlı akı zayıflama kontrolünün sağlanabileceği başarıyla gösterilmiştir. Ayrıca çalışma sonucunda KKG'nin daha iyi sonuçlar verdiği görülmüştür.

Anahtar Kelimeler Model öngörülü kontrol; Akı zayıflatma; Model referans adaptif sistem; Kayan kipli gözlemci; Doğrudan moment kontrolü.

1. Introduction

Electric vehicles are gaining popularity as a greener substitute for conventional fossil-powered automobiles (Global 2023). Low fuel costs and vehicle emissions are main benefits of electric vehicles, but their short driving range and lengthy charging times are their main drawbacks. In terms of lowering the greenhouse effect and resolving the energy issue, electric vehicles offer a significant benefit (De Santiago *et al.* 2011). Electric vehicles are expected to have a dynamic response, a high level of economy and torque, and dependability (Riba *et al.* 2016). Choosing the right motor, choosing the power electronic converter, and energy storage are the main

challenges for electric vehicles (Farasat *et al.* 2014; Mishra *et al.* 2022).

The choice of traction motor is influenced by various factors such as energy supply, fault tolerance, power density, efficiency, speed range, drive control flexibility, beginning torque, and driving cost per mile. In the context of electric vehicles traction requirements, permanent magnet synchronous motors, induction motors and brushless DC motors are common motor types. For electric vehicles, the induction motor is crucial since it complies with these requirements (Dias and Da Silva 2022). In addition, because of its simple design, simplicity of use, cheap maintenance costs, and durability,

induction motors are widely utilized in a wide range of industrial applications (Quintero-Manríquez et al. 2021, Emiroğlu 2023).

Direct Torque Control (DTC) is a control method used in AC motor drives to ensure high dynamic performance (Ren and Zhu 2014). It is a common control strategy for induction motors because of its ease of use, quick torque response, and resistance to changes in motor parameters (Alsofyani and Idris 2015). Furthermore, DTC eliminates the need for coordinate transformations, simplifying the control algorithm and lessening the computing load. This method chooses the optimal voltage vector for application to the motor by comparing the actual and reference values of torque and flux using hysteresis comparators. In this case, negative results such as high Total Harmonic Distortion (THD) value of stator current, high fluctuation in flux and torque, and difficulty in control at low speeds occur (Douiri and Cherkaoui 2013).

Flux weakening control strategy enables the motor's operational range to be expanded past its rated speed by reducing the magnetic flux in the rotor. A possible method for implementing flux weakening control is Model Predictive Control (MPC) (Zhang and Qi 2022). The MPC control approach makes use of a mathematical model of the system to predict future system behavior and optimize control measures accordingly (Gülbudak and Gökdağ 2022). MPC control reduces steady-state error when compared to other control methods (Alfaro et al. 2021). The MPC technique for flux weakening has only been applied in a very small number of experiments, and in these studies, the stator voltage or current d-axis component could be controlled (Chen et al. 2013; Su et al. 2017; Rubino et al. 2018). Because torque control in current controlled motor is implemented as an open loop, motor settings have a significant impact (Wang et al. 2015). Additionally, it responds slowly to changes in reference values (such as changes in speed or torque) (Rezgui et al. 2013).

The induction motor speed can be obtained using speed sensor in order to manage its speed and torque (Ammar et al. 2020). There are certain drawbacks to utilizing sensors to monitor speed in motor control, such as application challenges, high costs, and loud operation. There are drawbacks to using sensors in motor control, including application challenges, high costs, and noisy operation (Basar et al. 2013; Gómez-Peñate et al. 2019). Sensorless control of AC motors has therefore been suggested (Sengamalai et al. 2022). Different speed estimate techniques have so been put forth (Paicu et al. 2009). The most popular Sliding Mode Observer (SMO)

and Model Reference Adaptive System (MRAS) have been employed in this study. MRAS observer is based on a comparison of the stator currents or fluxes that are observed and those that are estimated (Jeong et al. 2014). An adjustable model and a reference model are used to generate the estimated values. Another important speed estimate technique that is simple to use, performs well, and has strong stability is the SMO (Ammar et al. 2017; Ye 2019). Additionally, it differs from other observers in that it does not require the speed and rotor time constant as inputs. The calculated fluxes and currents will remain unchanged regardless of changes to these values.

In this study, flux weakening control using MPC in DTC controlled induction motor is operated without speed sensor. The speed data required for the induction motor control has been estimated by two different methods which are SMO and MRAS observer. In this paper, the sensorless speed control performance of induction motor with MPC-based flux weakening control using SMO and MRAS have been evaluated. The current, speed (estimated and actual speed), flux and torque plots obtained consequence of the simulation research of the simulation study were evaluated. In addition, two estimation methods have been compared with stator currents THD values, flux and torque ripple amount and speed error values.

2. DTC of Induction Motor

As shown in Figure 1, the DTC block scheme for the induction motor is provided in a block design. In control scheme, induction motor driving system has 3 sections which are DTC, speed control and flux weakening control.

Voltage and current of the induction motor are kept track for DTC application. We use the observed voltage and current to calculate the motor torque, flux and flux sector. Flux and moment error values are evaluated with hysteresis comparators. The flux error is compared with a two-level comparator and the moment error is compared with a three-level comparator. As a result of the comparison, the control signal is obtained for both flux and torque. Using predicted flux sector and hysteresis controller signals, switching signals are determined and applied to power electronics switches in motor drivers.

Mathematical model of induction motor based on two axes system can be written as in Equations (1)-(6).

$$v_{sd} = R_s i_{sd} + \frac{d\psi_{sd}}{dt} - \omega_s \psi_{sq} \quad (1)$$

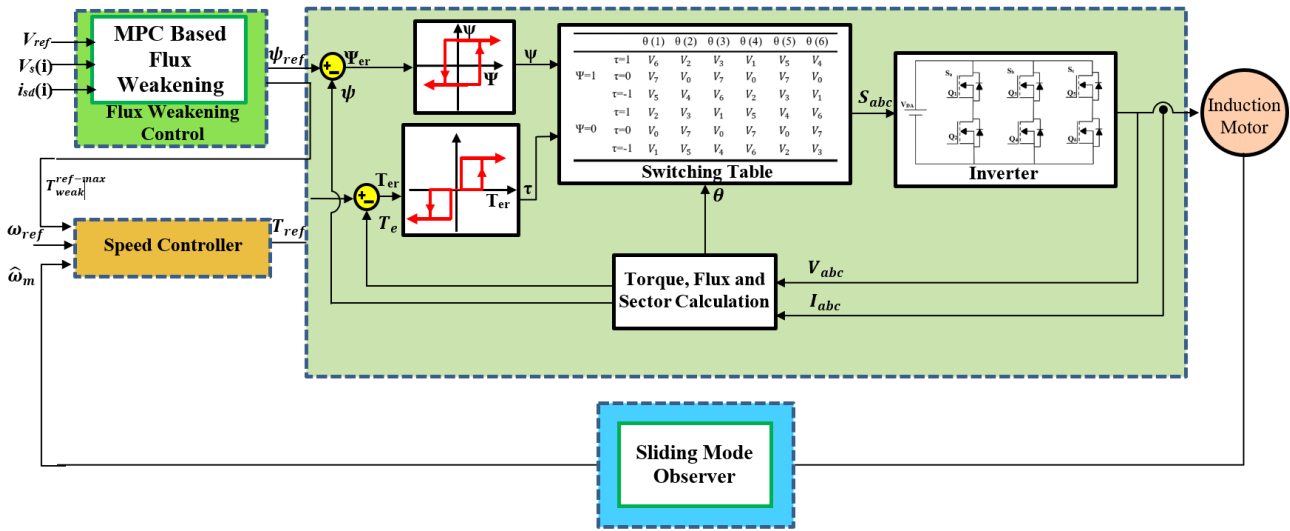


Figure 1. Block diagram of induction motor drive

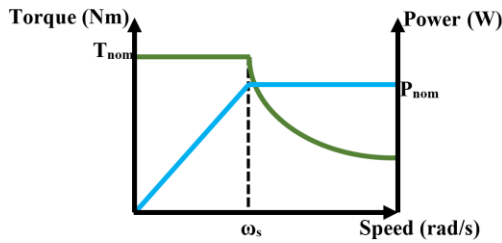


Figure 2. Induction motor power and torque characteristics for all speed range

$$v_{sq} = R_s i_{sq} + \frac{d\psi_{sq}}{dt} + \omega_s \psi_{sd} \quad (2)$$

$$\psi_{sd} = L_s i_{sd} + M i_{rd} \quad (3)$$

$$\psi_{sq} = L_s i_{sq} + M i_{rq} \quad (4)$$

$$T_e = p(i_{sq} \psi_{sd} - i_{sd} \psi_{sq}) \quad (5)$$

$$\omega_r = \frac{1}{B} \left(J \frac{d\omega_r}{dt} - T_e + T_l \right) \quad (6)$$

In (1)–(6), the terms two axes system (d and q-axis); stator and rotor current, stator voltage and stator flux are denoted by the following values: i_{sd} , i_{sq} , i_{rd} , i_{rq} , v_{sd} , v_{sq} , ψ_{sd} , ψ_{sq} .

The stator inductance and resistance, pole pair number, mutual inductance, inertia, load and induced torque, motor speed and friction are represented by the symbols: L_s , R_s , p , M , J , T_l , T_e , ω_r and B respectively.

3. Flux Weakening Control with MPC

Two different regions can be identified in speed control conjuncture of an induction motor by analyzing the speed-torque-power curve presented in Figure 2. This

region, as shown in Figure 2, is known as the constant torque region because there is a constant highest torque that can be achieved. In this region, the motor speed may be at or below its nominal value and in this region, the control process is performed with the current and voltage vectors of the motor. Motor speed exceeding the nominal speed is the other situation. Current or voltage vectors cannot be used for controlling induction motor because these values reach their nominal values once the motor comes to its nominal speed. In this area, the motor flux can be controlled in order to perform the control function. This area is known as the constant power region because, as Figure 2 illustrates, the motor power is constant there.

Flux weakening is required when running the motor at a speed greater than its nominal speed. The most prevalent and straightforward method for specification the flux reference at high speed is as follows in Equation (7).

$$\psi_{weak}^{ref} = \psi_{nom}^{ref} \frac{\omega_{nom}}{\omega_r} \quad (7)$$

In (7), the terms ω_{nom} and ω_r indicate rated and instant motor speed, ψ_{nom}^{ref} and ψ_{weak}^{ref} indicate flux references for constant torque and power region, respectively. Equation (8) can be utilized for calculating the torque limit in a manner similar to that of the flux reference.

$$T_{weak}^{ref-max} = -T_{weak}^{ref-min} = T_{nom}^{ref-max} \frac{\omega_{nom}}{\omega_r} \quad (8)$$

The upper value of the reference torque is denoted by $T_{nom}^{ref-max}$ in the preceding equation, and the higher and lower reference values of torque in the constant power zone are indicated by $T_{weak}^{ref-max}$ and $T_{weak}^{ref-min}$, respectively.

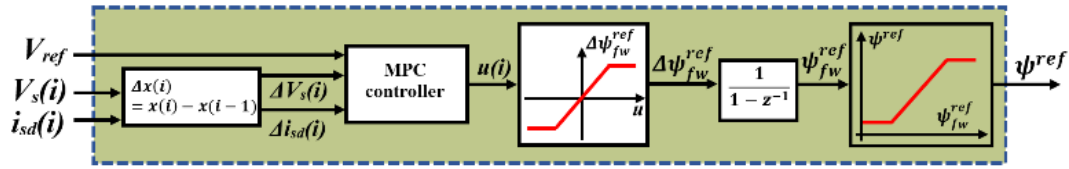


Figure 3. MPC based flux weakening control strategy

MPC has been used in this study to achieve better control performance in the region where flux is weakening. The flux weakening part of control scheme in Figure 1 is showed in greater detail in Figure 3.

The prediction model can be developed using the differential equations for the stator flux and current's d-axis components. The amount of variations in voltage is also taken into consideration. As seen in Equations (9) and (10), the d-axis component of stator flux, current, and voltage derivation in discrete time.

$$i_{sd}(i+1) = \left(1 - \frac{T_s}{\tau_c}\right) i_{sd}(i) + \frac{i_{sd}}{L_m \tau_c} \psi^{ref}(i) \quad (9)$$

$$\psi_{sd}(i+1) = \left(1 - \frac{T_s}{\tau_c}\right) \psi_{sd}(i) + \frac{T_s L_s}{\tau_r} \left(1 - \frac{\sigma \tau_r}{\tau_c}\right) i_{sd}(i) + \frac{\sigma T_s L_s}{L_m \tau_c} \psi^{ref}(i) \quad (10)$$

In the constant power region, for MPC based control of flux weakening, the steady-state model of the system can be expressed as in Equations (11) and (12).

$$x(i+1) = Ax(i) + Bu(i) \quad (11)$$

$$y(i) = Cx(i) \quad (12)$$

Here $x(i) = [\Delta i_{sd}(i) \Delta u_s(i)]$, $y(i) = u_s(i)$ and $u(i) = \Delta \psi_{az}^{ref}(i)$. Matrices A, B and C in Equations (11) and (12);

$$A = \begin{bmatrix} 1 - \frac{T_s}{\tau_c} & 0 \\ \frac{v_{sq}}{\sqrt{v_{sd}^2 + v_{sq}^2}} \frac{\omega_s T_s L_s}{\tau_r} \left(1 - \frac{\sigma \tau_r}{\tau_c}\right) & 1 - \frac{T_s}{\tau_r} \end{bmatrix}, \quad (13)$$

$$B = \begin{bmatrix} \frac{T_s}{\tau_c} \\ \frac{v_{sq}}{\sqrt{v_{sd}^2 + v_{sq}^2}} \frac{\sigma \omega_s T_s L_s}{\tau_c} \end{bmatrix}, \quad C = [0 \quad 1]$$

If Equations (11) and (12) are rewritten;

$$Y = \Phi Z(i) + \theta \Delta U(i) \quad (14)$$

$$\Phi = \begin{bmatrix} ME \\ ME^2 \\ \vdots \\ ME^{N_c} \end{bmatrix}, \quad (15)$$

$$\theta = \begin{bmatrix} MF & 0 & \cdots & 0 \\ MEF & MF & \cdots & 0 \\ \vdots & \vdots & \ddots & \vdots \\ ME^{N-1}F & ME^{N-2}F & \cdots & ME^{N-N_c}F \end{bmatrix}$$

Two of the most critical variables in the flux weakening area are upper reference value of voltage and flux. Therefore, it's critical to develop the cost function to reduce both the voltage reference-to-motor differential and the flux reference at the same time. MPC problem in the flux weakening area may be solved by formulating the system's cost function in Equation (16).

$$J_{cf} = \min \left(\sum_{n=1}^N \|P(i) - u_s(i+n)\|_2^2 + k_p \sum_{m=1}^{N_c} \|\Delta \psi_{weak}^{ref}(i+m-1)\|_2^2 \right) \quad (16)$$

Equation (16) is used for performing flux weakening control using the cost function.

4. Speed Estimation Methods

Due to the aforementioned drawbacks of sensor functioning, speed estimate techniques have been suggested in studies as a way to gather speed data without a sensor. Low cost and great dependability are offered by sensorless research. For speed estimate in this paper, MRAS and SMO were investigated.

4.1. Model Reference Adaptive System

The AC motor current model with speed is regarded as the induction motor adaptive model in the MRAS observer. The current model may be used to compute position and speed of rotor. The induction motor adaptive model may be expressed as in Equations (17) and (18).

$$\frac{di_{sd}}{dt} = \frac{1}{\sigma L_s} \left[-R_s i_{sd} + \sigma L_s \omega_s i_{sq} + \frac{L_m R_r}{L_r^2} \psi_{rd} + \omega_s \frac{L_m}{L_r} \psi_{rq} + V_{sd} \right] \quad (17)$$

$$\frac{di_{sq}}{dt} = \frac{1}{\sigma L_s} \left[-R_s i_{sq} - \sigma L_s \omega_s i_{sd} - \omega_s \frac{L_m}{L_r} \psi_{rd} + \frac{L_m R_r}{L_r^2} \psi_{rq} + V_{sq} \right] \quad (18)$$

Equations (19), (20) and (21) can be used to estimate speed .

$$\frac{di'_{sd}}{dt} = \frac{1}{\sigma L_s} \left[-R_s \hat{i}'_{sd} + \sigma L_s \omega_s \hat{i}'_{sq} + \frac{L_m R_r}{L_r^2} \psi_{rd} + \omega_s \frac{L_m}{L_r} \psi_{rq} + V_{sd} \right] \quad (19)$$

$$\frac{di'_{sq}}{dt} = \frac{1}{\sigma L_s} \left[-R_s \hat{i}'_{sq} - \sigma L_s \omega_s \hat{i}'_{sd} - \omega_s \frac{L_m}{L_r} \psi_{rd} + \frac{L_m R_r}{L_r^2} \psi_{rq} + V_{sq} \right] \quad (20)$$

$$\hat{\omega}_m = \int k_1(i'_d \hat{i}'_q - i'_q \hat{i}'_d) dt + k_2(i'_d \hat{i}'_q - i'_q \hat{i}'_d) + \hat{\omega}_m(0), k_1, k_2 \geq 0 \quad (21)$$

Here, ' indicates that the parameter is derived from an adaptive model and ^ indicates that the parameter is estimated.

4.2. Sliding Mode Observer

Since sliding mode is a changeable organization system, its reliance on the parameters of the system is quite low. The functioning of the sliding mode system is thus unaffected by uncertainties and disruptive forces inside the system. Stator resistance and rotor time constant are two examples of variables that change over time while AC motors operate. For improved control and reducing the negative effects of these variations during motor control, the sliding-mode structure is ideal.

An alternate approach for variable systems is sliding mode. The definition of a system with changeable structure is as follows. Additionally, the sliding surface (S) is described in the following description. In equations, the symbol \dot{x} denotes the derivative form of x.

$$\dot{x} = f(x, t, u), x \in R^n, u \in R^m \quad (22)$$

$$u = \begin{cases} u^+(x, t) & S(x) > 0 \\ u^-(x, t) & S(x) < 0 \end{cases} \quad (23)$$

$$S^T = (S_1, \dots, S_m) \quad (24)$$

Figure 4 demonstrates a sliding mode observer for induction motor. The following equations contain the induction motor current signals that can be examined by the observer.

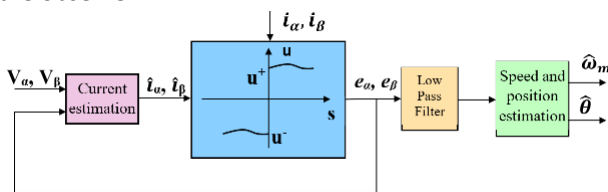


Figure 4. Sliding mode speed observer

$$\frac{d\hat{i}_\alpha}{dt} = \frac{1}{\sigma L_s} \left[-R_s \hat{i}_\alpha + \sigma L_s \omega_s f(\hat{i}_\alpha - i_\alpha) + \frac{L_m R_r}{L_r^2} \psi_{rd} + V_{sd} \right] \quad (25)$$

$$\frac{d\hat{i}_\beta}{dt} = \frac{1}{\sigma L_s} \left[-R_s \hat{i}_\beta - \sigma L_s \omega_s f(\hat{i}_\beta - i_\beta) + \frac{L_m R_r}{L_r^2} \psi_{rq} + V_{sq} \right] \quad (26)$$

Here, ^ indicates that variable is estimated. The discontinuous control block receives the estimated and

measured current values, and e_α and e_β control signals are produced.

$$e_\alpha = k_1 \text{sign}(\hat{i}_\alpha - i_\alpha) \quad (27)$$

$$e_\beta = k_1 \text{sign}(\hat{i}_\beta - i_\beta) \quad (28)$$

Here, k_1 is a positive gain. Equations (27) and (28) allow us to describe the sliding surface as following.

$$S = [s_\alpha \ s_\beta]^T = [\hat{i}_\alpha - i_\alpha \ \hat{i}_\beta - i_\beta]^T \quad (29)$$

According to Lyapunouv stability analysis;

$$V = \frac{1}{2} S^T S, V > 0 \quad (30)$$

$$\dot{V} = \frac{1}{2} S^T \dot{S}, \dot{V} < 0 \quad (31)$$

The low pass filter is applied to the resultant control signals (e_α and e_β), and the filter output values of e_α and e_β are then calculated. These values can be used to predict the rotor position and speed in the manner shown in Equations (32) and (33).

$$\hat{\theta} = -\tan^{-1}\left(\frac{e_\alpha}{e_\beta}\right) \quad (32)$$

$$\hat{\omega}_m = \frac{d\hat{\theta}}{dt} \quad (33)$$

5. Simulation Results

The speed control with sensorless method of DTC driven induction motor with MPC based flux weakening control is implemented in MATLAB m-file. For this reason, MATLAB is used for building the control system block diagram shown in Figure 1 utilizing the dynamic equations of an induction motor given in (1)-(6).

The block diagram showing the operation of the simulation program prepared in MATLAB is shown in Figure 5. As seen in the block diagram, the motor parameters given in Table 1 are first defined in the simulation program. The induction motor 3-phase currents are calculated with Equations (1)-(6). Using the calculated currents and voltage, the motor flux, torque and sector are calculated. After speed estimation with the sliding mode observer, moment is determined with the speed controller, flux reference is determined with the MPC, and the obtained signals are passed through the hysteresis controller. The appropriate voltage vector is determined using the sector and hysteresis controller outputs. The motor parameters utilized in the simulation study are listed in Table 1.

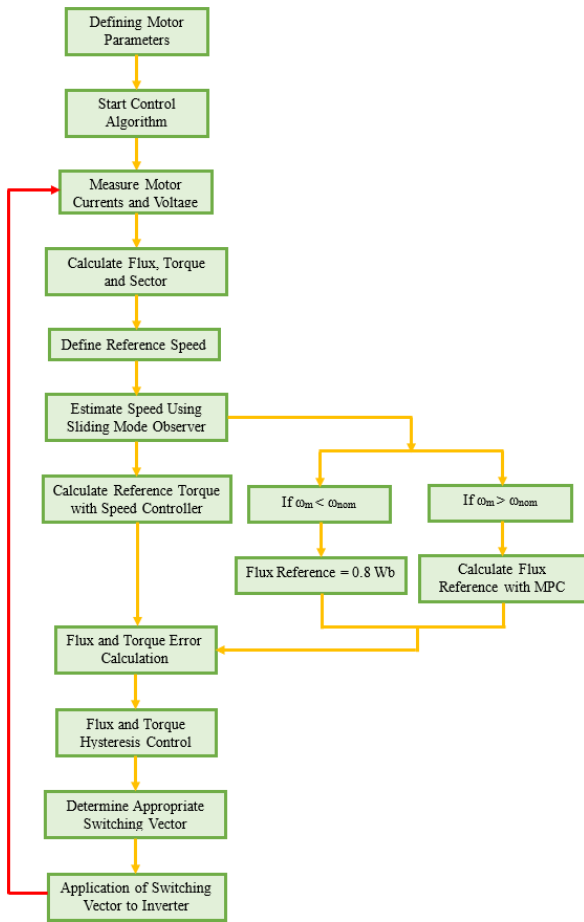
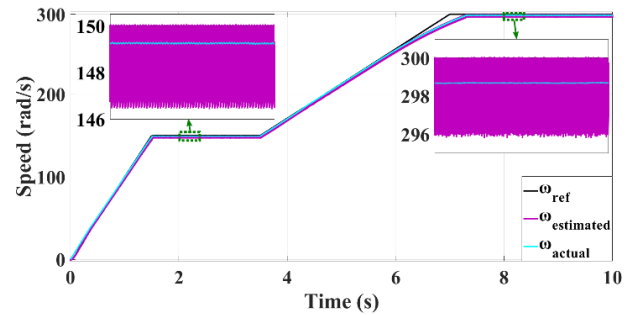


Figure 5. MATLAB simulation flowchart

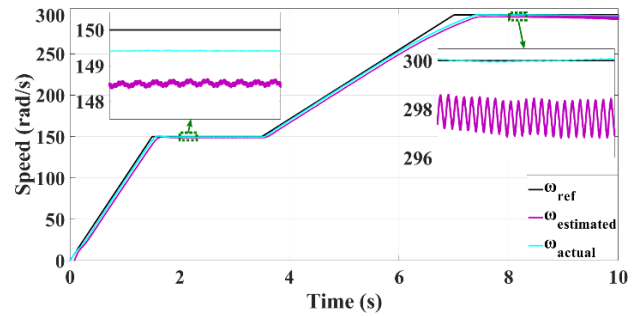
Table 1. Induction motor parameters

Parameter	Value
P	1,1 kW
R _s	7,7 Ω
L _s	0,0617 H
R _r	15,704 Ω
L _r	0,0617 H
R _c	882,42 Ω
L _m	0,04963 H
p	2
J	0,00689 kg m ²
B	0,00689 Nm-s/rad

The speed reference given in Figure 6 has been utilized. Figure 6 represents the sensorless speed performance of the DTC driven induction motor driver with MRAS and SMO. When examining the speed graph for MRAS, the estimated speed is quite fluctuating. The predicted speed fluctuation with SMO is less. When the graphs given in Figure 6 are examined, the effect of the fluctuation in the estimated speeds on the speed control performance is seen. Speed control performance is better with less fluctuation SMO. In addition, when the Root Mean Squared Error (RMSE) values for the nominal speed and flux weakening region given in Table 2 are examined, it is seen that SMO is more successful.



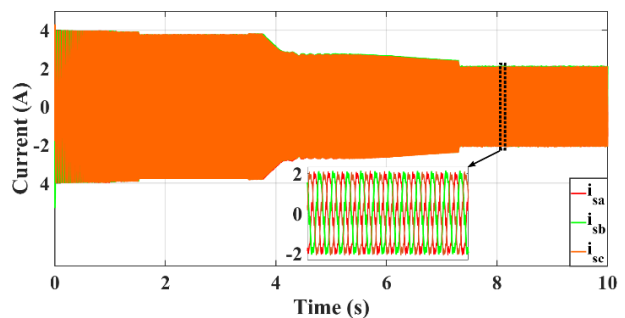
(a)



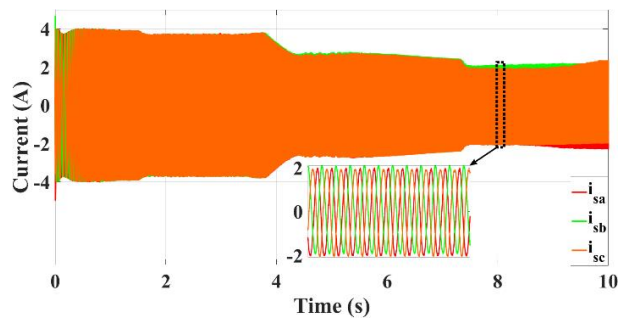
(b)

Figure 6. Speed performance of sensorless induction motor drive for (a) MRAS (b) SMO

Current graphs of DTC driven induction motor with MRAS and SMO are given in Figure 7. When analyzing the current graphs zoomed inside the flux weakening region, it becomes obvious there is a significant amount of current fluctuations with MRAS. When the THD values of the stator currents are examined, lower values are obtained in the MPC based flux weakening control region for the sensorless induction motor driver with SMO.



(a)



(b)

Figure 7. Stator currents of sensorless induction motor drive for (a) MRAS (b) SMO

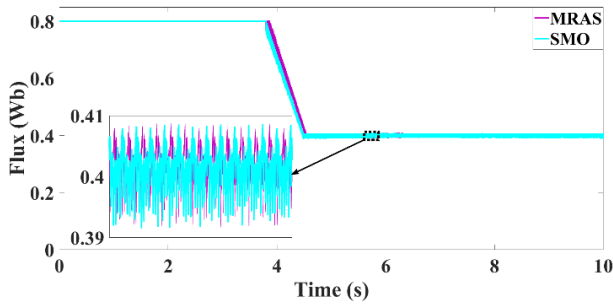


Figure 8. Flux of sensorless induction motor drive for MRAS and SMO

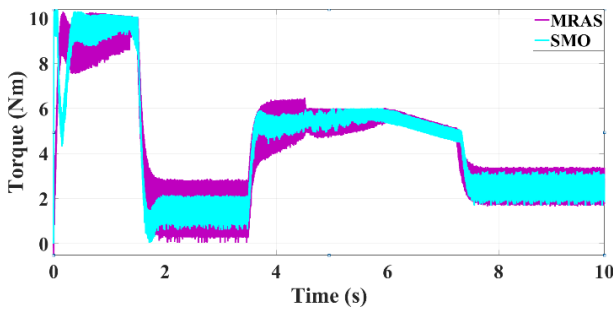


Figure 9. Torque of sensorless induction motor drive for MRAS and SMO

Flux and torque graphs for MRAS and SMO for speed sensorless induction motor drive are given in Figure 8 and 9, respectively. For SMO, there is less ripple in the torque plot in the rated speed and flux weakening regions. When the flux plot was examined, SMO has given a faster response. However, there was no significant change in flux fluctuation.

Table 2. Performance comparison for speed observers

Parameter	MRAS	SMO
THD _{isa}	8.5025	4.1979
THD _{isb}	8.9263	4.7204
THD _{isc}	8.9825	4.6073
RMSE _{nominal}	0.7409	0.5905
RMSE _{flux-weakening}	1.3105	0.3202

6. Conclusion

This study assesses an induction motor sensorless speed control capability using flux weakening control via MPC. The traction drive's overall performance, efficiency, and dependability are all negatively impacted by the use of speed sensors. Sensorless traction motor control offers dependable and incredibly effective performance. The speed required for speed control to be realized is estimated by MRAS and SMO. There are less speed errors with SMO when the speed graphs obtained by using the two speed estimating methods are analyzed. When comparing the two approaches, although there are no notable differences in terms of steady state ripple, upon examining the flux plot, SMO provides a more dynamic response. According to what is given in the Table 2, the performance of SMO is quite high, especially in the flux

weakening region. The performance obtained by using SMO has a positive effect on electric vehicle applications in terms of both precise speed adjustment and efficient operation. When the current, speed and torque graphs are evaluated, less ripple has been occurred with SMO. Low ripple in current, speed and torque causes low power loss during operation and provides energy efficiency in electric vehicle applications. When the THD values of the stator currents in the flux weakening region are examined, it is seen that SMO performs better than MRAS.

Declaration of Ethical Standards

The authors declare that they comply with all ethical standards.

Credit Authorship Contribution Statement

Author-1: Conceptualization, Methodology / Study design, Software, Validation, Formal analysis, Investigation, Resources, Writing – original draft, Writing – review and editing

Author-2: Conceptualization, Methodology / Study design, Software, Validation, Formal analysis, Investigation, Resources, Writing – original draft, Writing – review and editing

Declaration of Competing Interest

The authors have no conflicts of interest to declare regarding the content of this article.

Data Availability

All data generated or analyzed during this study are included in this published article.

7. References

- Alfaro C., Guzman R., de Vicuña L.G., Miret J., Castilla M., 2021. Dual-Loop Continuous Control Set Model-Predictive Control for a Three-Phase Unity Power Factor Rectifier. *IEEE Transactions on Power Electronics*, **37(2)**, 1447-1460. <https://doi.org/10.1109/TPEL.2021.3107221>
- Alsofyani I.M. and Idris N.R.N., 2015. Simple flux regulation for improving state estimation at very low and zero speed of a speed sensorless direct torque control of an induction motor. *IEEE Transactions on Power Electronics*, **31(4)**, 3027-3035. <https://doi.org/10.1109/TPEL.2015.2447731>
- Ammar A., Benakcha A. and Bourek A., 2017. Adaptive MRAC-based direct torque control with SVM for sensorless induction motor using adaptive observer. *The International Journal of Advanced Manufacturing Technology*, **91(5)**, 1631-1641. <https://doi.org/10.1007/s00170-016-9840-5>
- Ammar A., Kheldoun A., Metidji B., Ameid T. and Azzoug Y., 2020. Feedback linearization based sensorless direct torque control using stator flux MRAS-sliding mode observer for induction motor drive. *ISA Transactions* **98**, 382-392. <https://doi.org/10.1016/j.isatra.2019.08.061>
- Basar M.S., Bech M.M., Andersen T.O., Scavenius P. and Thomas-Basar T., 2013. *Comparison of sensorless FOC*

- and SVM-DTFC of PMSM for low-speed applications. Proceedings of 4th International Conference on Power Engineering, Energy and Electrical Drives. Istanbul, Türkiye, 864-869.
- Chen N., Zheng Z., Zhou J., Li Y. and Wang K., 2013. A novel MPC flux weakening method for induction motor applied in electric wheel. Proceedings of 2013 International Conference on Electrical Machines and Systems (ICEMS). Busan, South Korea, 113-118.
- De Santiago J., Bernhoff H., Ekergård B., Eriksson S., Ferhatovic S., Waters R. and Leijon M., 2011. Electrical motor drivelines in commercial all-electric vehicles: A review. *IEEE Transactions on vehicular Technology* **61(2)**, 475-484.
<https://doi.org/10.1109/TVT.2011.2177873>
- Dias C.G. and Da Silva L.C., 2022. Induction Motor Speed Estimation Based on Airgap Flux Measurement Using Hilbert Transform and Fast Fourier Transform. *IEEE Sensors Journal*, **22(13)**, 12690 - 12699.
<https://doi.org/10.1109/JSEN.2022.3176085>
- Douiri M.R. and Cherkaoui M., 2013. Comparative study of various artificial intelligence approaches applied to direct torque control of induction motor drives. *Frontiers in Energy* **7(4)**, 456-467.
<https://doi.org/10.1007/s11708-013-0264-8>
- Emiroğlu S., 2023. Parameter Estimation of Induction Motors using Hybrid GWO-CS Algorithm. *Sakarya University Journal of Science*, **27(2)**, 361-369.
<https://doi.org/10.16984/saufenbilder.1175899>
- Farasat, Mehdi, Andrzej M Trzynadlowski and Mohammed Sami Fadali, 2014. Efficiency improved sensorless control scheme for electric vehicle induction motors, *IET Electrical Systems in Transportation*, **4(4)**, 122-31.
<https://doi.org/10.1049/iet-est.2014.0018>
- Global E (2023) Global EV Outlook 2023: Catching up With Climate Ambitions.
- Gómez-Peñate S., Valencia-Palomo G., López-Estrada F.R., Astorga-Zaragoza C.M., Osornio-Rios R.A., Santos-Ruiz I., 2019. Sensor fault diagnosis based on a sliding mode and unknown input observer for Takagi-Sugeno systems with uncertain premise variables. *Asian Journal of Control*, **21(1)**, 339-353.
<https://doi.org/10.1002/asjc.1913>
- Gülbudak O. and Gökdağ M., 2022. Performance evaluation of model predictive control method for neutral point clamped inverter. *Turkish Journal of Engineering*, **6(3)**, 245-250.
<https://doi.org/10.31127/tuje.962857>
- Jeong I.W., Choi W. S. and Park K. H., 2014. Sensorless vector control of induction motors for wind energy applications using MRAS and ASO. *Journal of Electrical Engineering and Technology*, **9(3)**, 873-881.
<https://doi.org/10.5370/JEET.2014.9.3.873>
- Mishra, Saurabh, Anshul Varshney, Bhim Singh, and Hina Parveen, 2022. Driving-cycle-based modeling and control of solar-battery-fed reluctance synchronous motor drive for light electric vehicle with energy regeneration, *IEEE Transactions on Industry Applications*, **58(5)**, 6666-75.
<https://doi.org/10.1109/TIA.2022.3181224>
- Paicu M., Boldea I., Andreescu G.D. and Blaabjerg F., 2009. Very low speed performance of active flux based sensorless control: interior permanent magnet synchronous motor vector control versus direct torque and flux control. *IET electric power applications* **3(6)**, 551-561.
<https://doi.org/10.1049/iet-epa.2008.0290>
- Quintero-Manríquez, Eduardo, Edgar N Sanchez, M Elena Antonio-Toledo, and Flavio Muñoz, 2021. Neural control of an induction motor with regenerative braking as electric vehicle architecture. *Engineering Applications of Artificial Intelligence*, **104**, 1-14.
<https://doi.org/10.1016/j.engappai.2021.104275>
- Ren Y. and Zhu Z.Q., 2014. Enhancement of steady-state performance in direct-torque-controlled dual three-phase permanent-magnet synchronous machine drives with modified switching table. *IEEE Transactions on Industrial Electronics* **62(6)**, 3338-3350.
<https://doi.org/10.1109/TIE.2014.2376881>
- Rezgui S., Mehdi A., Legrioui S., Meddouche H., Boulahia A. and Benalla H., 2013. *IRFOC vs DTC performance comparison analysis*. Proceedings of 2013 3rd International Conference on Electric Power and Energy Conversion Systems. Istanbul, Türkiye, 1-6.
- Riba J.R., López-Torres C., Romeral L. and Garcia A., 2016. Rare-earth-free propulsion motors for electric vehicles: A technology review. *Renewable and Sustainable Energy Reviews* **57**, 367-379.
<https://doi.org/10.1016/j.rser.2015.12.121>
- Rubino S., Bojoi R., Odhano S.A. and Zanchetta P., 2018. Model predictive direct flux vector control of multi-three-phase induction motor drives. *IEEE Transactions on Industry Applications* **54(5)**, 4394-4404.
<https://doi.org/10.1109/TIA.2018.2829458>
- Sengamalai U., Anbazhagan G., Thamizh T.T., Vishnuram P., Khurshaid T. and Kamel S., 2022. Three Phase Induction Motor Drive: A Systematic Review on Dynamic Modeling, Parameter Estimation, and Control Schemes. *Energies* **15(21)**, 1-39.
<https://doi.org/10.3390/en15218260>
- Su D., Zhang C. and Dong Y., 2017. An improved continuous-time model predictive control of permanent magnetic synchronous motors for a wide-speed range. *Energies* **10(12)**, 1-18.
<https://doi.org/10.3390/en10122051>
- Wang Y., Shi Y., Xu Y. and Lorenz R.D., 2015. A comparative overview of indirect field oriented

control (IFOC) and deadbeat-direct torque and flux control (DB-DTFC) for AC Motor Drives. *Chinese Journal of Electrical Engineering* **1(1)**, 9-20.
<https://doi.org/10.23919/CJEE.2015.7933134>

Ye S., 2019. Fuzzy sliding mode observer with dual SOGI-FLL in sensorless control of PMSM drives. *Isa Transactions* **85**, 161-176.
<https://doi.org/10.1016/j.isatra.2018.10.004>

Zhang Y. and Qi R., 2022. Flux-weakening drive for IPMSM based on model predictive control. *Energies* **15(7)**, 1-14.
<https://doi.org/10.3390/en15072543>